Received: 16 June 2020 | Accepted: 17 June 2020

DOI: 10.1002/jez.2398

RESEARCH PAPER

JEZ-A ECOLOGICAL AND INTEGRATIVE PHYSIOLOGY WILEY

The control of routine fish maneuvers: Connecting midline kinematics to turn outcomes

Stephen P. Howe | Henry C. Astley

Department of Biology, Biomimicry Research and Innovation Center, University of Akron, Akron, Ohio

Correspondence
Stephen P. Howe, Department of Biology, Biomimicry Research and Innovation Center, University of Akron, 235 Carroll St., Rm D401, Akron, OH 44325-3908.
Email: stephen.p.howe@outlook.com

Abstract

Maneuverability is an important factor in determining an animal's ability to navigate its environment and succeed in predator–prey interactions. Although fish are capable of a wide range of maneuvers, most of the literature has focused on escape maneuvers while less attention has been paid to routine maneuvers, such as those used for habitat navigation. The quantitative relationships between body deformations and maneuver outcomes (displacement of the center of mass and change in trajectory) are fundamental to understanding how fish control their maneuvers, yet remain unknown in routine maneuvers. We recorded high-speed video of eight giant danios (*Devario aquepinnatus*) performing routine and escape maneuvers and quantified the deformation of the midline, the heading of the anterior body, and the kinematics of the centroid (a proxy for center of mass). We found that both routine and escape behaviors used qualitatively similar independent body bending events, which we curvature pulses, that propagate from head to tail but show quantitative differences in midline kinematics and turn outcomes. In routine maneuvers, the direction change and acceleration of the fish are influenced by both the magnitude of the bending pulse and by the duration of the pulse, whereas in escape maneuvers, only pulse duration influenced direction change and turn acceleration. The bending pulse appears to be the smallest functional unit of a turn, and can function independently or in combination, enabling a fish to achieve a wide range of complex maneuvers.

KEYWORDS

biomechanics, fish, kinematics, maneuverability, routine turns, swimming

1 | INTRODUCTION

Unsteady locomotion, such as turning and acceleration, is important for navigating complex environments, avoiding predators, and acquiring prey. Structurally complex habitats require increased maneuverability, defined as an animal's ability to change direction, encompassing both the extent of direction change and the space required to complete the maneuver (Gerstner, 1999; Walker, 2000). Success in predator–prey interactions often depends on agility, defined as the rate at which maneuvers are executed and the accelerations that an animal can generate, even at submaximal velocities (Howland, 1974; Moore & Biewener, 2015; Wilson et al., 2013; Wilson et al., 2018). Generally, pursuit predators are faster than their prey but prey tend to be more maneuverable (Howland, 1974; Wilson et al., 2018). In aquatic systems, maneuverability scales with size, smaller prey tending to be more maneuverable than large predators (Domenici, 2001; Vogel, 2008). An animal's capacity for steady or unsteady locomotion is reflected in its physiological, morphological, and behavioral adaptations. Short broad wings are better suited to birds and bats flying in confined spaces (Norberg & Rayner, 1987). Similarly, fish swimming in and around the complex reef structure have low aspect-ratio rounded pectoral fins and are more

 © 2020 Wiley Periodicals LLC

maneuverable than their more open-water neighbors (Gerstner, 1999). Mosquitofish in predation-heavy habitats also have deeper, more flexible bodies, and large low aspect-ratio caudal fins, which better suit them to unsteady swimming (Langerhans, 2009).

Terrestrial maneuvers involve an animal pushing against a solid substrate to change direction or accelerate, generating equal and opposite reaction forces at discrete contact points. In contrast, aquatic maneuvers require the animal to generate and interact with complex flows to impart momentum to the surrounding fluid. Fast starts are a family of behaviors that generally have shorter durations and higher accelerations (Webb, 1976) than routine swimming behaviors. They may be employed by fish in a number of situations including capturing prey (Webb & Skadsen, 1980), avoiding predators (Domenici & Blake, 1993; Hale, 2002; Liu & Hale, 2017) or perceived predators (Domenici et al., 2015), or during other high-energy behaviors (Webb, 1976). These rapid behaviors are observed in most fish and can be triggered reliably by startling the fish (Domenici & Hale, 2019; Eaton, Nissanov, & Wieland, 1984; Jayne & Lauder, 1993; Tytell & Lauder, 2002). Previous studies have examined the limits of muscle performance (Schriefer & Hale, 2004; Wakeling & Johnston, 1998; Westneat, Hale, McHenry, & Long, 1998), the behavior of the neuromuscular system (Dunn et al., 2016; Eaton & Emberley, 1991; Eaton, DiDomenico, & Nissanov, 1991; Eaton et al., 1984; Eaton, Lavender, & Wieland, 1981; Eaton, Lee, & Foreman, 2001; Foreman & Eaton, 1993; Jayne & Lauder, 1993; Tytell & Lauder, 2002), the kinematics (Domenici & Blake, 1991; Domenici & Blake, 1993; Fleuren et al., 2018; Weihs, 1973), and the hydrodynamics of the C-start (Weihs, 1973; Wu, Yang, & Zeng, 2007). Early papers describe escape responses as having preparatory and propagating phases (Gray, 1933; Jayne & Lauder, 1993; Weihs, 1973). These phases have since been described as stages of a double-bend maneuver (Domenici & Blake, 1993) and single-bend maneuvers have been observed (Domenici & Blake, 1993) which do not have the contralateral muscle activity (Tytell & Lauder, 2002) that defined earlier definitions of turn phases. Multiple papers have shown that fish can accelerate during both stages of the escape response (Fleuren et al., 2018; Tytell & Lauder, 2008). Escape responses can vary in speed depending on the type of stimulus and the physical conditions (Domenici & Batty, 1994; Domenici & Hale, 2019; Domenici, Standen, & Levine, 2004; Meager, Domenici, Shingles, & Utne-Palm, 2006). In some high-performing species including pike, angelfish, and knifefish, these maneuvers total heading changes can exceed 180 degrees, accelerations can exceed 100 m/s^2, and turning radii are as small as 6% of the body length (Domenici & Blake, 1997). The range and diversity of escape maneuver types likely contributes to the continued success of fishes in aquatic environments.

Routine maneuvers, such as those used in habitat navigation, have been examined less often (Budick & O'Malley, 2000; Domenici et al., 2004; Wu et al., 2007). Budick and O'Malley (2000) found that routine and escape turns could be readily distinguished by their turning rate, this difference has been repeatedly observed and is used to distinguish between routine and escape maneuvers (Domenici et al., 2004; Dunn et al., 2016; Ghisleni et al., 2012; Meager et al., 2006). Wu et al. (2007) focused mainly on the effects of turning rate on kinematics and hydrodynamics, and found that routine turns have similar kinematic stages as escape maneuvers, having both preparatory and propagating phases, with most of the heading change occurring in the first phase of the turn. The wakes of fast turns have thrust jets associated with Stage 1 that are not found in slow turns (Wu et al., 2007). Schrank, Webb, and Mayberry (1999) and Webb and Fairchild (2001) conducted experiments with fish constrained by channels and free swimming and found that the fish beat their tails asymmetrically. In both studies, fish were chased by the experimenters, and thus, while the maneuvers were probably not Mauthner-mediated C-starts, they could hardly be described as routine.

To achieve effective locomotor control, fish must be able to relate the deformations of their bodies to the resulting changes in direction and speed. However, the detailed kinematics—the body deflections that fish undergo during routine maneuvers, and how those deflections are modulated to control turn outcomes—remain unknown. In most cases, the body kinematics reported were simple, such as the deflection of the tail from an hypothetical body axis (Jayne & Lauder, 1993; Webb, 1978; Wu et al., 2007), or the angle between the head and tail (Voesenek, Pieters, Muijres, & van Leeuwen, 2019). In zebrafish larvae, turn angle is correlated with body curvature and turn speed is correlated with duration of the maneuver (Voesenek et al., 2019). Eaton et al. (2001) found a relationship between the number of neurons involved in the escape response and the heading change of the fish, but they did not describe how changes in body shape correlated to those changes in heading. While the tail is important in generating and directing flow, the highly flexible body is likely to also contribute to the kinematic outcomes of the maneuver. We will be describing the following three features of the fish maneuvering system: (a) the behavior of the midline, how it develops and propagates bending; (b) the performance outcomes of the turn, for example, how fast the fish changes direction and velocity; and (c) the relationships between midline kinematics and performance outcomes.

2 | METHODS

We used eight adult giant danios (*Devario aquepinnatus*; McClelland, 1839), with a mean length from rostrum to the base of the central caudal fin ray of 46.3 ± 3.9 mm. Pairs of individuals swam together in still water in a 76-L glass tank (61.6 cm × 31.8 cm × 32.4 cm), because lone fish exhibited signs of stress and would not behave normally. We used visual implant elastomer tags (Northwest Marine Technology Inc., Anacortes, WA) to identify individuals. These tags were implanted subdermally at various positions on the dorsum of the fish. As we were recording ventral videos, the tags could not be used to identify the fish in the video; however, we paired individuals with different size which allowed us to identify individuals in the video. A mirror set at 45 degrees beneath the tank allowed us to capture the ventral view of the fish. The fish were backlit using a

light-emitting diode (LED) light table (Porta-Trace 1824 LED lightbox, Gagne Inc., Johnson City, NY) placed above the tank. We recorded video at 500 frames/s and a shutter speed of 1/1,000th second using an Edgertronic SC1 color high-speed video camera (Sanstreak Corp., San Jose CA; Supporting Information Video).

We included 150 turns in our analysis, using three methods to incite turning behaviors. As our primary interest is routine turns, most turns ($N = 100$) involved no stimulus from the experimenter. To provide comparison to these, we used two different methods of startling fish to attempt to trigger escape responses through multiple sensory pathways and thereby increasing the diversity of escape responses: visual stimuli (the experimenter waving their hands in front of the tank, $N = 17$) and percussive stimuli (the experimenter tapping on the walls of the tank out of view of the fish, $N = 33$). During preliminary analysis, we found that turns across all treatments clustered into two main groups across many variables (Figure 3), which precluded standard regression analysis. We decided to group the data using a *K*-means cluster analysis of all midline and turn outcome variables instead of by treatment, as the behavioral outcomes were more informative than the stimulus type, and the clustering analysis allowed us to split visually stimulated turns in a robust way. The variables in the cluster analysis are scaled individually. The *K*-means cluster analyses separated most turns without stimuli (96/100) and most turns with a percussive stimulus (26/33) into the two groups, with turns due to visual stimuli split between them (12 and 5, respectively). These clusters are based on and correspond to our original experimental treatment. The cluster that contains mostly turns without stimuli we call "routine maneuvers," whereas "escape maneuvers" are the cluster that contains mostly turns with percussive stimuli. There were several cases where the *K*-means algorithm "miscategorized" turns. In the case of percussive turns, we found that these miscategorized turns were often turns that occurred before the main stimulated turn and would have in other circumstances been categorized as voluntary.

Videos were processed using a custom MATLAB code (MathWorks, Inc., Natick, MA; Supporting Information Material). Each frame was subjected to a series of morphological operations to approximate the midline of the fish. The color image (Figure 1a) was desaturated and inverted (Figure 1b). The desaturated image was subject to a gradient filter, which detected the edges of the fish better than thresholding and produced a binarized outline (Figure 1c). The binarized outline generated by the gradient filter was then filled (Figure 1d). We identified which object was the fish from the first frame and then automatically tracked the movements of the fish throughout the rest of the video. The binarized image was smoothed using a gaussian blur filter to reduce irregularities that could lead to spurs forming during the skeletonization step (Figure 1e). The binary image was skeletonized using the "thin" option in the MATLAB function bwmorph (Figure 1e). Fins or other objects sticking out form the fish silhouette can give rise to a spur off the backbone. We included a despurring module that could identify and remove spurs and loops in the midline. Skeletonizing an image reduces the length of the midline because the operation eliminates the outermost pixels with more than two neighbors. It can be several iterations before a pixel is isolated on an end of the fish, and as a result, the total length of the fish will be shortened. To compensate for this, the midline was extended by linearly extrapolating the ends of the midline back to the edges of the binary image of the fish using the slopes of the head and tail regions (Figure 1e). The resulting line was then smoothed with a cubic spline using the MATLAB function spaps (Figure 1f) with parameters chosen to balance fidelity to the raw backbone and elimination of kinks and other errors in the backbone reconstruction. The spline was weighted to anchor the head and tail and the tolerance was set to two thirds the length of the fish in pixels. We calculated radius of curvature for each point along the backbone by fitting a circle to three points: the target point and two additional points located a fixed distance anterior and posterior to the target point. The center of the circle is found by finding the intersection of the two lines created by the three points. The inverse of the radius of that circle is the geometric distance to any of the sample points. This distance was set to 7% of the fishes' body length, approximately the length of three vertebrae, for a total span of six vertebrae. This assumes the fishes head constitutes 15% of the body length and the remaining 85% is divided between 35 vertebrae (values obtained from dissection of three fish). The inverse of the radius of curvature is reported as curvature and is normalized by

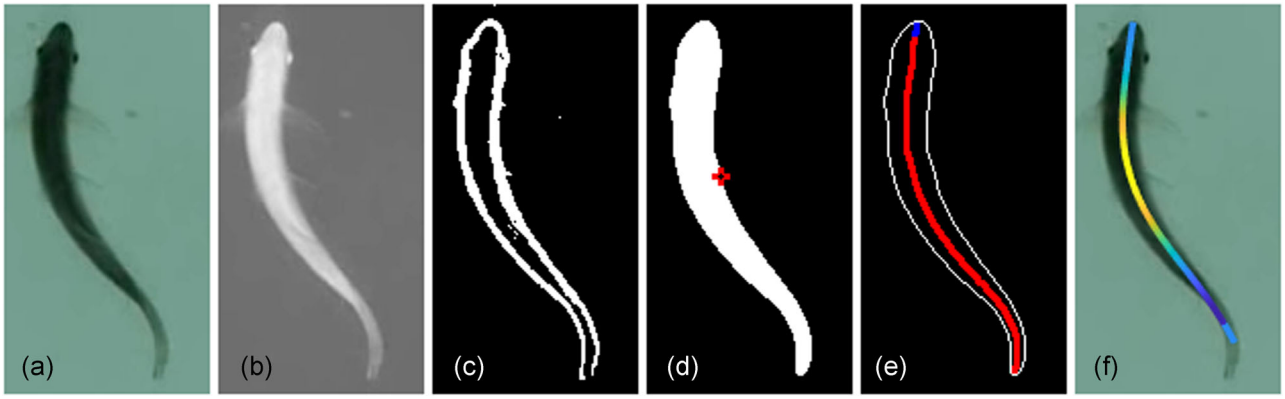

FIGURE 1 Image analysis montage [Color figure can be viewed at wileyonlinelibrary.com]

body length. We chose to use curvature instead of deflection as in Jayne and Lauder (1993) and Wu et al. (2007). Measuring deflection requires establishing a midline axis from which to measure deflection. In straight swimming systems, this is easier, but as fish are turning this would require reorienting the midline axis as the fish turns based on either head orientation or average body orientation, each of which entails certain assumptions. Curvature is an internally consistent measure of body bending which does not require a whole-body geometric landmark. Right handed curvature was assigned positive values and left-handed curvature negative values.

To better characterize the independent nature of turning behaviors, we treat regions of body bending as traveling peaks of curvature as opposed to continuous waveforms. At any time during the turn, curvature peaks at some point on the body and decreases toward both the head and the tail. This peak evolves over time as the amplitude, width, and position of the peak change over the course of the turn. Taken together, these individual curvature peaks form a "pulse" of curvature that travels down the body over time. We define a curvature "pulse" as the area (Figure 2a) of positive or negative curvature that describes the initiation, growth, propagation, and termination of curvature on the body (Supporting Information Video). To limit noise we used Otsu's method (Otsu, 1979; MATLAB function: graythresh) to set a minimum curvature threshold (0.48·BL^{-1}) to measure pulses averaged across all videos. Pulses that exceeded this global curvature threshold were counted as maneuvers, distinct from steady swimming behaviors. Many of the maneuvers captured were complex and consisted of multiple sequential or overlapping pulses. We categorized a given pulse as "primary" if it did not co-occur on the body with another pulse or was the first in a series. We define "secondary" pulses as one following a primary pulse and overlapped in time. We restricted our analysis to primary pulses; which constitute pulses that do not overlap in time with any other pulse, or the first in a series of overlapping pulses ($N = 31$). We made this decision because we found significant kinematic differences that between primary and secondary pulses that complicate the results and are outside the scope of this paper. The kinematics of these "first of a series" pulses were significantly different from "stand alone" pulses; however, the magnitude was small and the overall analysis was unchanged if they were excluded. We therefore decided to retain these pulses in the analysis. Secondary pulses, however, had large kinematic differences compared to primary or first of a series pulses. Composite maneuvers, defined as multiple pulses in series, sometimes overlapping in time, are described qualitatively in the discussion.

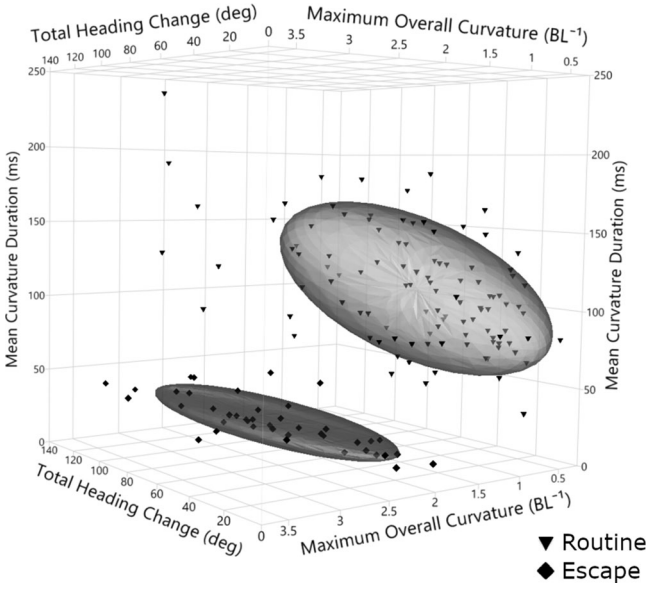

FIGURE 3 Three-dimensional performance space showing data clustering

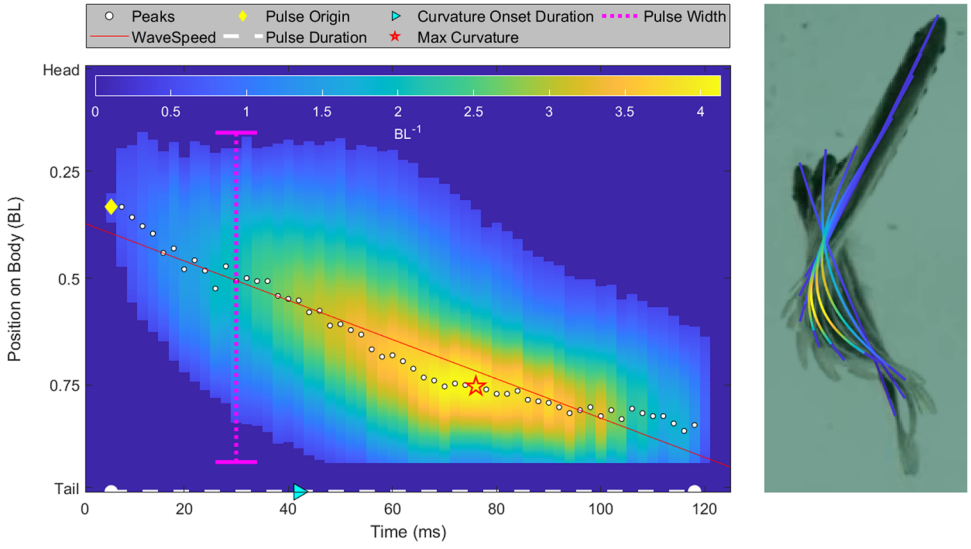

FIGURE 2 Pulse measurements [Color figure can be viewed at wileyonlinelibrary.com]

We used eight kinematic variables to characterize individual pulses (Figure 2a): maximum curvature, maximum overall curvature, pulse duration, mean curvature duration, mean pulse width, pulse speed, curvature onset duration, and pulse origin. Maximum curvature is simply the maximum body curvature attained at any time during the pulse. Maximum overall curvature computes the average curvature on the fish's body during a frame and finds the maximum value over the duration of the turn. This metric accounts for how much of the body is engaged; values below the curvature threshold are set to zero and included in the averaging calculation, bringing down the average curvature as less of the body is engaged in the pulse. Maximum overall curvature is similar to tailbeat amplitude in steady swimming systems, head to tail angle (Voesenek et al., 2019), or minimum moment of inertia (Fleuren et al., 2018), in that it gives a measure of how tightly the whole body is bent during a turn. Curvature variables are reported as the inverse of body lengths (BL^{-1}). Pulse duration is the time elapsed from the first frame the midline curvature crosses the threshold to the last frame that curvature is above the threshold. Mean curvature duration is the average time each point along the body axis achieves a curvature greater than the threshold, that is, the average horizontal width of the enclosed region in Figure 2a. In steady swimming systems, these variables would be similar to tailbeat frequency. We include mean curvature duration because it better approximates how long each body segment is active and may correlate with muscle activation durations. Mean pulse width is an average of the fraction of the body that is greater than the curvature threshold over the duration of the turn, that is, the average vertical height of the enclosed region in Figure 2a. Small mean pulse widths indicate that curvature is very localized on the body, whereas large mean pulse widths indicate the curvature is spread out along more of the body. Pulse speed was calculated as the slope of a linear regression of the position of peak curvature on the body as a function of time. Some turns had short regions of no propagation before and after the main phase of propagation. We excluded these regions when calculating the slope of the regression. Curvature onset duration is the time it takes the peak curvature to achieve 80% of the maximum curvature for the pulse. We report curvature onset duration as a percentage of pulse duration, as the raw curvature onset duration will likely covary with pulse duration and we are interested more in how much of the pulse is spent building curvature. Pulse origin is the position of the peak curvature on the body in the first frame of the pulse (Figure 2a). Duration variables are reported in ms while all length based variables and their time derivatives are normalized by BL.

Prior papers have tracked the center of mass by determining the location of the center of mass of a straight fish and tracking this point on the midline (a third to halfway along the midline; Jayne & Lauder, 1993; Webb, 1983; Westneat et al., 1998). The center of mass represents the average location of all mass in the body, and forces are typically represented acting upon the center of mass. When highly curved, the center of mass of the fish may move outside the body, and bending motions may cause discrepancies between the movement of the body axis and the motion of the center of mass, making it crucial to accurately track to assess outcomes such as linear and centripetal acceleration. Recent studies (Fleuren et al., 2018; Voesenek et al., 2019) have been fitting three-dimensional reconstructions of the fish to their video data, which has allowed for direct tracking of the center of mass directly during the turn. We have elected to track the centroid of the ventral image as a proxy for center of mass to approximate its behavior (Supporting Information Video). We approximated the position of the center of mass kinematics using the centroid of the binarized image of the fish during image analysis (Figure 1c). A similar method was used in Tytell and Lauder (2008) where the true center of mass position was approximated using the reconstructed midline and the length specific mass of the fish. The centroid of an image of a fish when straight was 41% of the length of the fish, which is in agreement with prior papers (Jayne & Lauder, 1993; Webb, 1983; Westneat et al., 1998). We smoothed the path of the centroid using a cubic spline (MATLAB function: csaps), and measured velocity, centripetal and linear acceleration, and the direction of the centroid motion. The smoothing parameter (p) started at .0001 and could be increased to better fit the centroid path. We used a csaps for the path of the centroid instead of spaps because it was better at handling certain errors that resulted from artificially high curvatures of the path induced by centroid jitter. To calculate the heading of the fish, we used the first point of the midline and a point 15% of the length of the fish to calculate the heading of the fish. This distance was within cranial region of the fish, which is effectively rigid. These points were also smoothed using csaps ($p = .0001$) before being used in heading calculations.

We report two heading change metrics: total heading change and maximum instantaneous heading change; and six centroid metrics: maximum centroid velocity, maximum linear acceleration and centripetal acceleration of the centroid, minimum radius of curvature, total angular centroid displacement (the angular difference of the velocity vector of the centroid), and maximum instantaneous angular centroid displacement. Heading change variables are based on the angular displacement of the head between successive frames. Maximum instantaneous heading change is the largest angular displacement between successive frames over the course of the turn. Total heading change is the sum of all the angular displacements over the whole turn. Centroid variables are based on the linear displacement of the centroid between successive frames. We used the diff function in MATLAB to get the approximate derivative of the smoothed X and Y centroid position data. Maximum velocity is the largest linear displacement of the centroid between two frames. Angular centroid displacement is the angular difference between two successive velocity vectors. This metric requires three frames, the first and second frame define the reference velocity vector and the second and third frames define a new vector that may or may not have a different orientation relative to the prior vector. Acceleration is similarly numerically approximated from the X and Y velocity components obtained in the previous step. Linear acceleration is the component of the acceleration vector colinear with the velocity vector of the centroid. It is calculated by taking the dot product of the velocity unit

vector and the acceleration vector. Centripetal acceleration is the component of the acceleration vector that is perpendicular to the velocity vector. It is calculated by taking the dot product of the unit vector perpendicular to the velocity vector and the acceleration vector. The minimum turn radius is found by fitting a circle fit to three sequential points along the path of the centroid in the same manner as described for calculating curvature of the midline. We follow the convention of prior authors (Domenici, 2001; Vogel, 2008) by reporting acceleration as m/s^2 squared. All other metrics are size normalized using BL.

2.1 | Statistics

After collecting and clustering the data, we found that two of the eight individuals did not perform routine maneuvers and three of the eight individuals did not perform escape maneuvers. In tests that directly compare routine and escape maneuvers, we only used the three individuals that performed both types of maneuvers. In tests where we were not quantitatively comparing routine and escape maneuvers, namely the linear mixed models, we included all individuals that contributed more than four turns to the cluster. Table 1 summarizes the participation of each individual in each statistical test. All statistical tests were performed in JMP 14 (SAS Institute, Inc., Independence, OH).

Preliminary analysis showed substantial covariation within both the midline and the turn outcome variables. We conducted separate principal component analysis (PCA) for both the midline kinematics and the turn outcome kinematics for routine ($N = 108$) and escape maneuvers ($N = 42$), resulting in four separate PCAs. JMP standardizes variables as part of the analysis. We used these analyses to identify major groupings of variables and choose representatives from among them. We did not use the rotated components in our linear models as the factor loadings made the interpretation of the components difficult. Based on eigenvalues, we found that most of the variation in our midline kinematic data set could be explained by two factors for both routine and escape maneuvers. Similarly, the majority of the variation in turn outcome variables could be explained in two factors for routine maneuvers. Escape maneuvers had three axes with eigenvalues greater than 1, but as we are focusing on routine maneuvers, we chose to narrow our focus to two factors. We performed a factor analysis for two factors using principal components as the factoring method and prior communality, and rotated the factors using the varimax method. In both routine and escape PCAs, the factor loadings were similar (Table 3). In the midline PCA, the factor loadings showed similar patterns in routine and escape maneuvers. One factor loaded primarily curvature-related variables and the other loaded primarily duration-related variables. In routine turns, the curvature factor explained more of the variation than the duration factor, and the opposite was true for escape maneuvers. For clarity, we flipped the factor numbering in escape turns so that factor 1 in both routine and escape turns refers to the factor strongly loading curvature and factor 2 refers to the factor strongly loading duration. We chose maximum overall curvature as the representative variable for midline factor 1 and mean curvature duration as the representative variable for the midline factor 2. The turn outcome factors were also similar between routine and escape maneuvers. One factor loaded primarily direction change variables, hereafter outcome factor 1 and the other loaded primarily velocity change variables, hereafter outcome factor 2. We chose total heading change and maximum centripetal acceleration as the representative variables for the turn outcome factors. We tried to balance biomechanical relevance and the different loadings between routine and escape maneuvers, weighing routine maneuvers more heavily as we are focusing on routine maneuvers in this paper. As such, the representative variables may not be the highest loading variables on their given axes. Choosing a consistent set of representative variables across routine and escape maneuvers allows us to qualitatively compare the linear mixed models generated for each treatment.

We fit a total of four linear mixed models, one for each turn outcome variable in both routine and escape clusters. The starting effects included the full factorial set generated from the two midline kinematic variables and individual as a random effect. We ran the models with unbounded variance components, which in JMP calculates the confidence intervals for the random effect covariance estimates using Wald-based methods. The interaction between mean active duration and maximum average curvature was not significant in either of the routine models and only one of the escape models. We decided to remove that interaction term and the third-order interaction with individual from all the models for consistency. Our final model included mean active duration and maximum average curvature as fixed effects and individual and its interactions with the

TABLE 1 Number of trials per individual and included in the different statistical tests

Individual identifier	Escape	Routine	Total
2	0	30	30
3	6	10	16
4	13	2^+	15^+
5	10	29	40
7	4	0	4^+
8	6	9	15
9	3^+	24	27^+
10	0	4	4^+
Total	42	108	150
N (linear mixed model)	35	102	
N (standard least squares)	24	39	63

Note: The table lists the individuals by their number, we had some individuals that were not included in the analysis entirely. The total number of trials used in the clustering analysis was 150. Trials marked with + were excluded from the standard mixed model analysis. The standard least squares analysis used turns from individuals 3, 5, and 8 and excluded eight visually stimulated turns.

mean active duration and maximum average curvature as random effects. We excluded trials from individuals contributing less than five turns and log transformed all variables entering the model.

Three individuals had significant numbers of turns in both treatments. To compare treatments, we fit a standard least squares analysis on the original treatments instead of the clusters using trials from individuals three five and eight. We excluded visually stimulated turns and contrasted voluntary turns and percussive. Visually stimulated turns only had eight turns split (5/3) between escape and routine maneuvers. One percussive turn was excluded as it occurred before the main turn in its video and would have otherwise been coded as voluntary. Excluding them did not significantly reduce the sample size or remove turns in a biased way. We would like to reiterate that the models described here use the a priori treatment groups voluntary turns and percussively stimulated turns. The model was constructed including treatment, individual, and the treatment individual interaction. The results of those 16 tests were Bonferroni corrected and are reported in Table 2.

In the course of our statistical analysis, we tried multiple different methodologies, all of which provided qualitatively similar results; the analyses we have chosen present our data in a comprehensive yet concise format. We also provide the full data set in the Supporting Information Material (Table S1) and source videos and code are available through data dryad (see DataDryad link in the Acknowledgments section).

3 | RESULTS

We observed a wide range of maneuvers ($N = 150$) with heading change ranging from 1.7 to 138 degrees (mean: 50.24, *SD*: 30.52) and durations from 30 to 326 ms (mean: 124.16, *SD*: 62.20). Maximum body curvature ranged from 1.28 to 7.87·BL^{-1} (mean: 3.84, *SD*: 1.51) and maximum velocity ranged from 1.19 to 30.06 BL/s (mean: 6.88, *SD*: 6.34). Maximum centripetal acceleration ranged from 0.14 to 50.73 m/s^2 (mean: 7.37, *SD*: 11.42) and maximum linear acceleration ranged from −0.3 to 56.11 m/s^2 (mean: 7.79, *SD*: 12.99). Reynold's number ranged from 2,361 to 65,415 with a (mean: 15,586, *SD*: 14,252). These statistics cover the entire range of data. Means and standard deviations for the voluntary and percussive turns are found in Table 2.

Midline deformations during turns consist of pulses of curvature that originate at a point near the midpoint along the body (46.4 ± 10.5% of the body length from the anterior) and propagate from head to tail (Figure 2 and Supporting Information Video). After initiation, curvature increases both toward the head and the tail as more of the fish's body becomes involved in the pulse (Figure 2).

TABLE 2 Differences in kinematic variables between routine turns and C-starts

		Percussive ($N = 24$)				Voluntary ($N = 39$)				Whole model	
	DF = 5, 57 Variable	Min	Mean	*SD*	Max	Min	Mean	*SD*	Max	F-ratio	*p* > F
Midline kinematics	Mean curvature duration (ms)	14.51	42.66	33.94	153.47	29.00	111.49	44.37	190.64	13.80	**<.0001***
	Maximum overall curvature (BL^{-1})	0.82	2.33	0.56	3.56	0.48	1.27	0.74	2.75	14.31	**<.0001*,X**
	Maximum curvature (BL^{-1})	1.83	5.33	1.16	7.40	1.65	3.14	1.52	7.87	15.60	**<.0001*,X**
	Pulse origin (% BL)	0.29	0.41	0.09	0.67	0.32	0.51	0.12	0.69	5.47	**.0004***
	Curvature onset duration (% pulse duration)	0.16	0.34	0.06	0.47	0.27	0.39	0.08	0.55	4.93	**.001***
	Mean width (% BL)	0.43	0.58	0.11	0.76	0.32	0.55	0.14	0.71	1.22	.31
	Wave speed (BL/s)	2.24	13.74	4.36	27.08	0.75	2.91	5.70	15.04	22.44	**<.0001***
	Pulse duration (ms)	30.00	64.92	42.60	186.00	46.00	154.82	55.69	232.00	14.99	**<.0001***
Turn outcomes	Total heading change (deg)	4.09	66.74	30.06	138.28	1.77	40.38	39.31	120.52	5.33	**.0004*,X**
	Maximum centripetal acceleration (m/s^2)	0.89	17.38	7.05	37.82	0.18	1.34	9.22	21.96	18.20	**<.0001i,X**
	Maximum instantaneous heading change (deg/s)	225.75	2091.18	754.03	4719.75	96.64	622.64	985.88	1944.17	15.52	**<.0001i,*,X**
	Maximum velocity (BL/s)	2.38	13.51	3.33	25.35	1.59	3.18	4.36	9.39	32.52	**<.0001i,X**
	Maximum path curvature (BL^{-1})	1.30	11.53	11.94	88.85	0.67	3.02	15.62	11.74	2.28	.059*
	Maximum instantaneous angular displacement (deg/s)	428.39	2563.09	976.71	5109.21	90.77	434.62	1277.04	3474.89	15.80	**<.0001***
	Maximum linear acceleration (m/s^2)	−0.30	19.12	8.60	52.10	0.10	1.05	11.25	14.56	16.07	**<.0001i,***
	Total angular displacement (deg)	9.81	69.13	26.30	119.63	7.25	38.37	34.39	112.57	6.02	**.0002*,X**

Note: DF = (5, 82). The whole model *p*-values were Bonferroni corrected. Bold values are given where treatment is significant. Superscript (i) indicates individual was significant, superscript (*) indicates treatment was significant and superscript (^{X}) indicates when the interaction was significant.
Abbreviation: *SD*, standard deviation.

After approximately a quarter of the pulse duration, the curvature begins to decrease at the head and progresses toward the tail as the body unfurls (Figure 2). We found that the peak curvature on the body started propagating toward the tail almost immediately and with a largely constant velocity (Figure 2).

The two PCAs of midline kinematics in routine and escape clusters each revealed two factors accounting for a total of 67.49% and 58.36% of the variation in routine and escape maneuvers, respectively (Table 3). In routine and escape maneuvers, the midline factor 1 had strong loadings of curvature variables and midline factor 2 loaded primarily variables related to duration (Table 3). Midline factor 1 accounted for a greater portion of the variation in routine maneuvers whereas midline factor 2 accounted for more variation in escape maneuvers. Maximum overall curvature, the representative for its factor, loads very highly on the curvature factor in both routine and escape turns. In routine turns it loads minimally on the duration factor, whereas it has a higher, though not strong, loading on the duration factor in escape maneuvers (Table 3). Mean curvature duration, the representative for midline factor 2, loads very high on the escape midline factor 2 and very low on midline factor 1. Mean curvature duration is the second highest loaded factor on the routine midline factor 2, with a moderate loading on midline factor 1 (Table 3). The two PCAs for the turn outcomes identify two major factors that account for a total of 78.5% and 68.21% of the variation for routine and escape maneuvers, respectively (Table 3). Total and instantaneous heading change, angular displacement, and minimum turn radius loaded strongly on outcome factor 1 (Table 3). Linear and centripetal acceleration as well as velocity loaded highly on outcome factor 2 (Table 3). Though the axes are from different analyses, the factor loadings were similar and consistent between routine and escape maneuvers. Total heading change, the representative variable for outcome factor 1, had the second highest loading on its factor and the lowest off-factor loading in routine maneuvers. In escape maneuvers, total heading change had the third highest on-factor loading and the lowest off-factor loading. Maximum centripetal acceleration, the representative variable for outcome factor 2, had the highest on-factor loading and lowest off-factor loading in both routine turns and loaded moderately on both axes in escape turns.

The linear mixed model predicting total heading change in routine turns found no significant covariation with individual or its interactions with the fixed effects (akaike information criterion [AICc]: 129.83; Table 4). The model predicting maximum centripetal acceleration in routine maneuvers found significant covariations in all the random effects but only individual*mean curvature duration had a large covariation estimate relative to the total (AICc = 99.07). Mean curvature duration had a significant negative effect on maximum centripetal acceleration, whereas maximum overall curvature had a significant positive effect (Figure 4 and Table 5). Only maximum overall curvature had significant positive effects on total heading change (Figure 4). The model predicting total heading change in escape maneuvers found a relatively large effect of individual*maximum overall curvature (AICc = 43.95). Only mean

TABLE 3 Factor loading matrix for routine and escape maneuvers for the midline kinematics PCA and the turn outcomes PCA

	Midline kinematic variables			Turn outcome variables		
	Factor	**1**	**2**	**Factor**	**1**	**2**
Escape	*Eigenvalues*	1.52	3.15	*Eigenvalues*	*3.27*	*2.19*
	Mean curvature duration (seconds)	**0.02**	**0.97**	**Total heading change (deg)**	**0.89**	**−0.07**
	Maximum overall curvature (BL^{-1})	**0.81**	**0.37**	**Maximum centripetal acceleration (m/s^2)**	**0.30**	**0.46**
	Maximum curvature (BL^{-1})	0.81	0.02	Maximum instantaneous heading change (deg/s)	0.93	0.10
	Pulse origin (% BL)	0.49	−0.20	Maximum velocity (BL/s)	−0.27	0.79
	Curvature onset duration (% pulse duration)	−0.39	−0.18	Maximum path curvature (BL^{-1})	0.01	0.56
	Mean width (% BL)	−0.06	0.69	Maximum instantaneous angular displacement (deg/s)	0.55	0.65
	Wave speed (BL/s)	−0.33	−0.78	Maximum linear acceleration (m/s^2)	−0.51	0.79
	Pulse duration (seconds)	0.13	0.78	Total angular displacement (deg)	0.91	−0.18
	Percent variation explained	22.82	35.54	*Percent variation explained*	*40.13*	*28.08*
Routine	*Eigenvalues*	*3.00*	*2.40*	*Eigenvalues*	*4.68*	*1.56*
	Mean curvature duration (seconds)	**0.46**	**0.84**	**Total heading change (deg)**	**0.92**	**0.13**
	Maximum overall curvature (BL^{-1})	**0.95**	**0.05**	**Maximum centripetal acceleration (m/s^2)**	**0.29**	**0.91**
	Maximum curvature (BL^{-1})	0.84	−0.01	Maximum instantaneous heading change (deg/s)	0.86	0.42
	Pulse origin (% BL)	−0.51	0.36	Maximum velocity (BL/s)	−0.07	0.93
	Curvature onset duration (% pulse duration)	0.22	−0.50	Maximum path curvature (BL^{-1})	0.74	−0.02
	Mean width (% BL)	0.72	0.07	Maximum instantaneous angular displacement (deg/s)	0.83	0.48
	Wave speed (BL/s)	0.27	−0.86	Maximum linear acceleration (m/s^2)	0.26	0.53
	Pulse duration (seconds)	0.35	0.83	Total angular displacement (deg)	0.92	0.19
	Percent variation explained	*35.79*	*31.70*	*Percent variation explained*	*47.89*	*30.61*

Note: The variables we chose to represent each factor are bolded. Italics indicate the values are summary statistics and not variables.
Abbreviations: BL, body length; PCA, principal component analysis.

curvature duration had a significant positive effect (Figure 4 and Table 4). The model predicting maximum centripetal acceleration in escape maneuvers had significant covariations in all the random effects but only individual maximum overall curvature had a large covariation estimate relative to the total (AICc = 45.98). Neither fixed effect had a significant conditional effect on maximum centripetal acceleration.

Almost all variables showed significant differences between voluntary (routine) and percussive (escape) maneuvers. The only variables that were not significantly different between treatments were mean pulse width and maximum path curvature (Table 2). Maximum velocity was four times greater and maximum linear acceleration was 13 times greater in escape responses compared to routine maneuvers (Table 2). Mean curvature duration was nearly four times longer in routine compared to escape maneuvers (Table 2). There were some cases were individual or the interaction between individual and treatment was significant. The differences between midline kinematic variables and turn outcome variables are summarized in Table 2 with means and standard deviations.

4 | DISCUSSION

Two important and widely used metrics of a maneuver are the magnitude of directional change (maneuverability) and speed of directional change (agility; Webb, 1994). Maneuverability has been represented by variables like turn angle (Domenici & Blake, 1993; Voesenek et al., 2019) or minimum turn radius (Blake, Chatters, & Domenici, 1995; Domenici & Blake, 1991; Webb, 1983; Webb, 1976). Agility has been represented by variables like maximum velocity (Voesenek et al., 2019), acceleration (Fleuren et al., 2018; Tytell & Lauder, 2008; Webb, 1983), and turning rate (Chadwell, Standen, Lauder, & Ashley-Ross, 2012; Domenici & Blake, 1993). We found that turn outcome variables grouped into two factors which broadly correspond to maneuverability and agility, respectively (Table 3). The only major loading difference between routine and escape maneuvers is that maximum centripetal acceleration loads strongly on centroid PC2(R) but does not load strongly on either centroid PC axis in escape maneuvers (Table 3). This strongly supports considering maneuverability and agility as separate and largely independent turn outcomes.

The midline of the fish is a high degree of freedom system theoretically capable of many complex postures and motions through time. However, during turning, many variables that describe the deformation of the midline during the turn collapse into two orthogonal axes related broadly to the curvature of the pulse and the duration of the pulse. The strongest loading factors on midline factor 1(R & E) and midline factor 2 (R & E) were curvature- and duration-related variables, respectively (Table 3). Pulse speed loads negatively on midline factor 2 (R & E) in both escape and routine maneuvers, which is to be expected as pulse speed is a function of both pulse origin and pulse duration (Table 3). Curvature onset duration loads

TABLE 4 Summary statistics of the total heading change linear mixed models

DFNUM = 1	Total heading change					
Escape	Variance component			Estimate	*SE*	Wald *p*
	Individual			−0.012	0.003101	.0001
	Individual*Log [mean curvature duration (ms)]			1.85	1.80	.30
	Individual*Log [maximum overall curvature (BL^{-1})]			2.25	0.59	**.0001**
	Residual			0.15	0.04	
	Total			4.25	1.87	
	Source	Estimate	*SE*	DFDen	F-ratio	Prob > F
	Log [mean curvature duration (ms)]	1.79	0.25	3	51.30	**.0056**
	Log [maximum overall curvature (BL^{-1})]	0.52	1.76	30	0.09	.77
Routine	Variance component			Estimate	*SE*	Wald *p*
	Individual			0.02	0.03	.46
	Individual*Log [mean curvature duration (ms)]			−0.03	0.08	.72
	Individual*Log [maximum overall curvature (BL^{-1})]			0.11	0.16	.49
	Residual			0.17	0.03	
	Total			0.31	0.17	
	Source	Estimate	*SE*	DFDen	F-ratio	Prob > F
	Log [mean curvature duration (ms)]	0.31	0.15	2.3	4.37	.16
	Log [maximum overall curvature (BL^{-1})]	1.55	0.22	2.9	49.13	**.0066**

Note: Random and fixed effects are reported bolded values are significant after Bonferroni correction.
Abbreviation: *SE*, standard error.

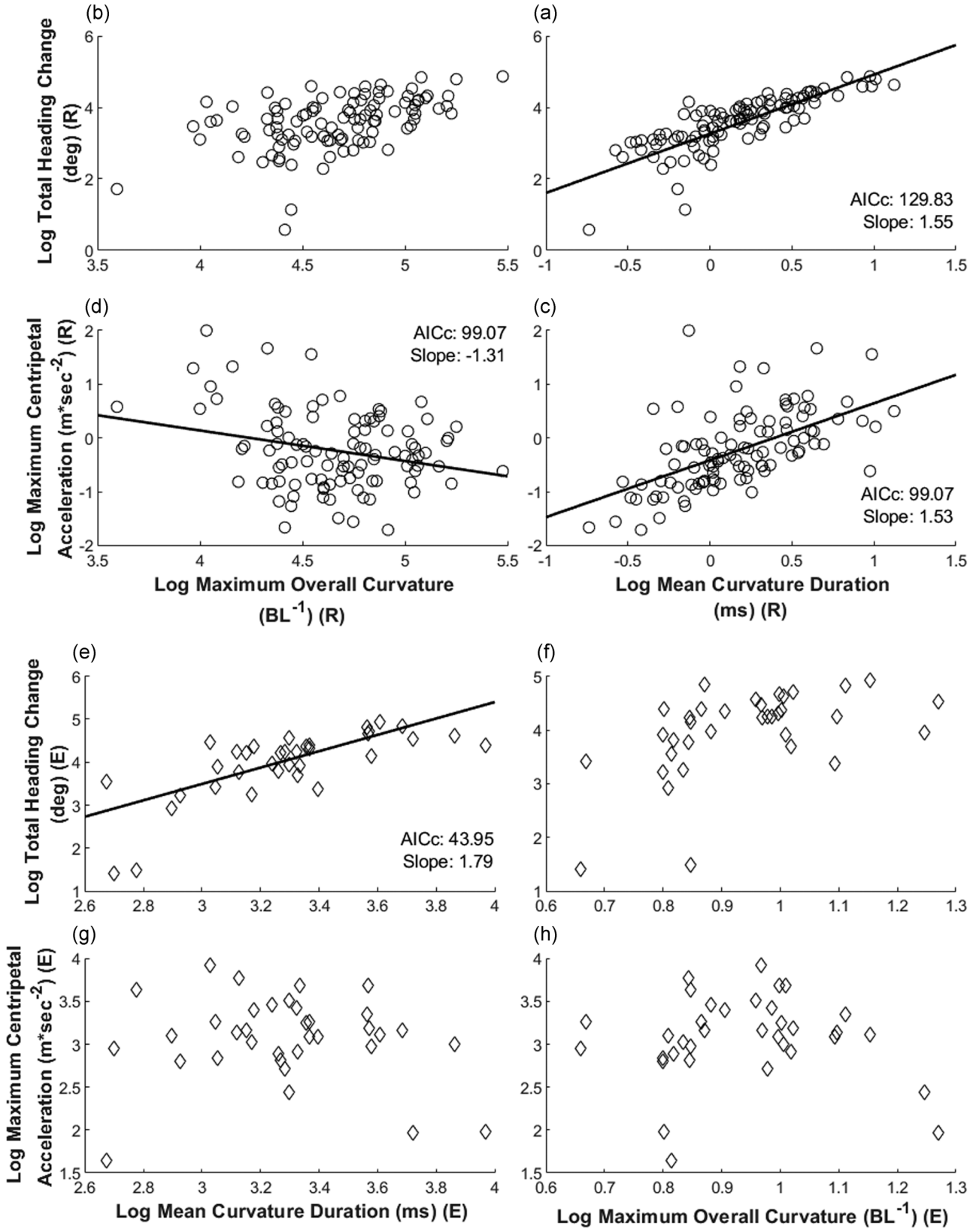

FIGURE 4 Linear model plots between midline kinematics and turn performance. Akaike information criterion (AICc) given for each significant model.

TABLE 5 Summary statistics of the maximum centripetal acceleration linear mixed models

DFNUM = 1	Maximum centripetal acceleration					
Escape	Variance component			Estimate	*SE*	Wald *p*
	Individual			0.002	0.0004	<.0001
	Individual*Log [mean curvature duration (ms)]			−0.006	0.001	<.0001
	Individual*Log [maximum overall curvature (BL^{-1})]			−0.98	0.25	**<.0001**
	Residual			0.26	0.07	
	Total			0.26	0.07	
	Source	Estimate	*SE*	DFDen	F-ratio	Prob > F
	Log [mean curvature duration (ms)]	−0.30	0.37	32	0.66	.42
	Log [maximum overall curvature (BL^{-1})]	0.06	0.29	32	0.04	.85
Routine	Variance component			Estimate	*SE*	Wald *p*
	Individual			−0.01	0.00	<.0001
	Individual*Log [mean curvature duration (ms)]			0.09	0.01	<.0001
	Individual*Log [maximum overall curvature (BL^{-1})]			−0.01	0.00	**<.0001**
	Residual			0.17	0.02	
	Total			0.26	0.04	
	Source	Estimate	*SE*	DFDen	F-ratio	Prob > F
	Log [mean curvature duration (ms)]	−1.31	0.30	98.1	19.74	**<.0001**
	Log [maximum overall curvature (BL^{-1})]	1.53	0.07	99	496.19	**<.0001**

Note: Random and fixed effects are reported bolded values are significant after Bonferroni correction.
Abbreviation: *SE*, standard error.

negatively on midline factor 2(R) but flips and loads negatively on midline factor 1 in escape turns (Table 3). This shows that curvature onset duration takes a smaller fraction of the overall duration of the turn as pulse duration increases. Neither mean pulse width nor pulse origin loaded strongly on either midline factor 1(E) or midline factor 2(E) in escape maneuvers. Pulse origin loads negatively on midline factor 2(R) (Table 3) which indicates that pulse origin moves closer to the head as curvature increases involving more of the body in the propagation of the pulse. Mean pulse width loads positively on midline factor 2(R) (Table 3), which indicates that more of the body is involved in the pulse as curvature increases, spreading the curvature over more of the body. While midline factor 1(R & E) generally relates to pulse duration and midline factor 2(R & E) generally relates to curvature and body dynamics, it is important to note that though duration loaded the strongest on midline factor 1(R) it had a significant loading on midline factor 2(R) (Table 3). This correlation between duration and curvature variables is only seen in the routine turns. Taken together, these results show that, despite the wide range of possible midline deformations, the fish are using a relatively consistent pattern of deformation which is primarily modulated by the intensity of the curvature and the duration of the pulse.

We elected to fit models using representative variables from each factor instead of testing the composite factors themselves. Routine turns have a number of conditional effects active in their control. Body curvature has strong positive effects on both centripetal acceleration and heading change (Figure 4). As the body bends tighter the head deflects more, the fish also changes its angular momentum allowing it to rotate about its center of mass. The fish is then able to unfurl its body without reversing the heading change it achieved during the height of the pulse. Tighter body curvatures leading to faster turns is likely due to the fish being able to entrain and accelerate more water (Akanyeti et al., 2017). Fish need to be able to turn in all directions, at many different speeds. Mean curvature duration has a strong negative conditional effect on acceleration (Figure 4), which allows fish to modulate their speed independent of their directional change. Mean curvature duration did not have a significant effect on total heading change in routine maneuvers. However in escape maneuvers, mean active duration has a positive conditional effect on heading change. This indicates a limit to how quickly a fish can reorient. This has implications for decision making in escape behavior. The extra time it takes to turn farther may reduce a fishes chances of escape. Mean curvature duration does not appear to have a significant effect on acceleration in escape maneuvers as it does in routine maneuvers. Maximum overall curvature appears to not affect escape maneuvers in any way. Preliminary analysis using a free swimming robotic model programed to approximate the midline kinematics we observe here are consistent with the control relationships we observed the live fish (Howe & Astley, in preparation). Voesenek et al. (2019) found that zebrafish larvae escape response heading change is predominately controlled by body curvature and velocity is controlled by pulse duration. However, in adult fish, Domenici and Blake (1991) and Eaton, DiDomenico, and Nissanov (1988) found that turn angle and turn duration were correlated in angelfish and goldfish. It is interesting that larval zebrafish have control relationships that bear more resemblance to the control of routine maneuvers we have seen in adult

giant danios, but the escape response control relationships we observed in giant danio are more similar to those of other adult fish. More studies that directly compare the kinematics of maneuvering throughout ontogeny and across species would help understand the differences we observed in the control relationships.

Our kinematic results concur with previous studies comparing the behaviors of escape responses and routine maneuvers (Wu et al., 2007). The difference between these maneuvers is quantitative more than qualitative. Both types of maneuvers have a pulse origin slightly anterior to midbody which progresses posteriorly as curvature increases rostrally and caudally, and finishes with the curvature returning to zero as the wave propagates from head to tail. The quantitative differences between routine and escape maneuvers we observed are in agreement with earlier studies (Budick & O'Malley, 2000; Domenici et al., 2004; Dunn et al., 2016; Meager et al., 2006). Escape maneuvers are generally shorter and have higher velocities and accelerations.

When mean curvature duration and maximum curvature are plotted against one another we can start to identify trends in the performance space available to giant danios (Figure 5). In the previous section, we discussed the correlation between duration and curvature in routine maneuvers and noted there was no similar relationship in escape maneuvers. This correlation in routine maneuvers may be due to an imbalance in the use of performance space. There is a distinct absence of low curvature long duration turns that may be driving the correlation between these variables. The short duration, higher curvature routine turns are edging closer to escape response range. Others have shown that slow escape responses are part of a fish's maneuverability repertoire (Domenici & Hale, 2019; Domenici et al., 2015; Meager et al., 2006) and we would expect to see the lines blur between escape and routine maneuvers. As of yet we do not have a mechanistic or physiological principle in mind that would explain the absence of low duration low curvature turns. It is very likely that this is a behavioral artifact and we would need many more trials and possibly different conditions to show these lower limits on fish turning performance. We found some indications that escape and routine maneuvers may be on a broader continuum, however we were not focusing on escape maneuvers and thus have neither the sample size nor range of behaviors (e.g., the slow escape responses described in Domenici & Hale, 2019) to say anything on the universality of these control relationships.

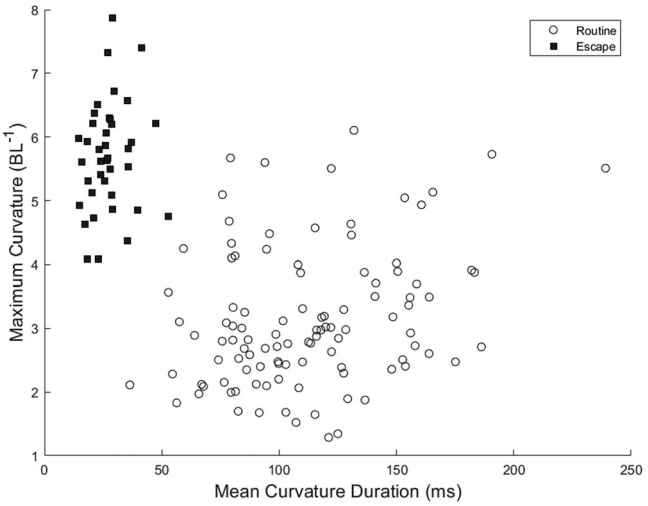

FIGURE 5 Curvature versus duration performance space

The clustering in our data is apparent in Figures 3 and 5. Escape turns are very short and have the highest curvatures of all maneuvers. Routine turns are longer and have much lower curvatures. Muscle physiology may be responsible for the patterns of use in the performance space. Time is the important variable distinguishing escape and routine maneuvers. As maneuver duration decreases muscles must contract at higher velocities, and thus muscle force decreases (Hill, 1938). Fish recruit different muscle fiber types to maintain power at high velocities: red muscle is used for low velocity, efficient maneuvers whereas white muscle is used for high power, high velocity motions (Rome et al., 1988). In our data set, the delineation between routine and escape maneuvers occurs around 50 ms mean active duration. This is the same contraction duration where Jayne and Lauder (1994) found that steady swimming fish transition from predominately red muscle use, for slow swimming, to white muscle use, for fast swimming. On the other hand, routine maneuvers appear to have a curvature ceiling of $6{\cdot}BL^{-1}$ even though the maximum curvature value we observed over all trials is closer to $8{\cdot}BL^{-1}$. The red muscle in giant danios (Biga & Goetz, 2006) may not be strong enough to overcome both the hydrodynamic force of the water and the resistive forces imposed by the body's own tissue to achieve higher curvatures in those durations. These relationships are likely to change among species of fish that have different muscle fiber compositions and anatomical arrangements. More targeted electromyographical and anatomical studies would be required to test whether and how muscle physiology delimits the maneuverability performance space.

Instead of being limited by the range of midline parameter values and outcomes of a single pulse, the existing literature and our data both show that fish can increase the complexity of maneuvers by combining multiple pulses (Figure 6). There appear to be kinematic differences between initial and subsequent pulses. Preliminary examination suggest secondary pulses in both routine and escape maneuvers appear to engage less of the body (i.e. smaller pulse width), originate closer to the head, and have shorter durations than primary pulses. We observed several classes of composite maneuvers that deserve further study. Fish can power wider turns by using multiple asymmetrically strengthened pulses (Figure 6a,b), similar to the asymmetric tail beats observed in (Webb & Fairchild, 2001). We found pairs of pulses in which fish were able to initiate new pulses without waiting for previous pulses to conclude. Figure 6c shows a strong right pulse overwhelming a smaller left-handed straight swimming pulse between 50 and 100 ms. A left-handed pulse follows this right handed pulse which resembles the two stages of a double-bend turn described in (Domenici & Blake, 1993). A maneuver we repeatedly observed pairs two pulses of opposite sign. This results in the fish performing a “sidestep” in which the fish moves forward and

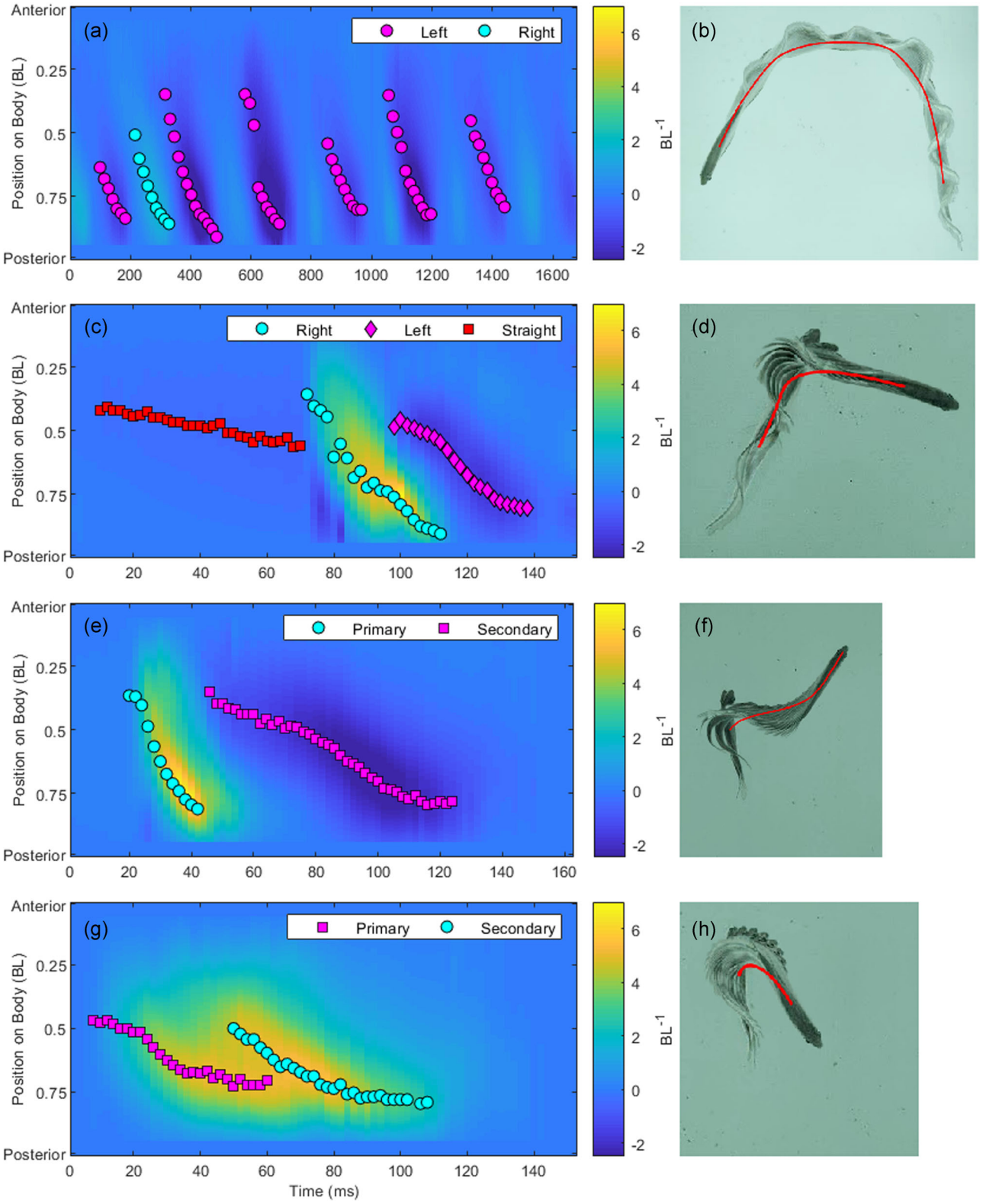

FIGURE 6 Curvature map and centroid paths for various compound maneuvers [Color figure can be viewed at wileyonlinelibrary.com]

laterally with an overall heading change less than either individual pulse (Figure 6e,f). Like the previous example this turn consists of two stages, though the magnitude of the second stage is strong enough to cancel some of the heading change achieved during the first pulse. In addition, fish can stack pulses of the same sign. We have seen multiple examples of fish overlapping pulses of the same sign to various degrees. In the most extreme cases a turn that appears to be a single pulse has two peaks of curvature that propagate down the body (Figure 6g,h). Combining pulses would allow fish to achieve greater total acceleration, and control the acceleration while maintaining a desired heading, while also providing opportunities for course correction.

A single turn with unusually small radius of curvature values demonstrates the limitations of radius of curvature as a metric for defining maneuverability. Radius of curvature is commonly used to refer to the space required to complete a maneuver, and is usually measured using the path of the center of mass (Blake et al., 1995; Domenici & Blake, 1991; Webb, 1983; Webb, 1976). In most cases, this measure is accurate, particularly when the body in question is largely rigid and the turning radius is much greater than body length. However, in the case of flexible bodies, the center of mass (and our centroid) often lies outside the body (Voesenek et al., 2019). In one observed turn, we found that the combination of body deflection, speed, and reorientation timing was able to produce a turn with near zero minimum radius of curvature of the centroid path ($0.01 \cdot BL^{-1}$; Figure 7). Walker (2000) discusses a similar phenomenon in box fish, which have rigid body. Rigidity is normally associated with reduced maneuverability (Fish, 1999), but these fish can complete turns of zero radius (Walker, 2000). More rigid swimmers compensate for these physical limitations to achieve the very small turning radii by using different behaviors or including other fins in their turning system (Downs, Block, & Fish, 2019; Fish, 1999). As turn radius approaches zero, the space required to complete a turn becomes more important (Walker, 2000: Figure 7). Schrank et al. (1999) quantified this metric by reducing the width of a bent channel constraining the fish until failure. While maneuvering in confined spaces is an important system to study, those same walls may interfere with the hydrodynamics of the system. Modern digital tracking algorithms allow the space occupied by the body during the turn to be easily computed (Figure 7). Comparing normalized space requirements for turns would allow for better comparisons of maneuverability between fish in situations where turn radius is very small.

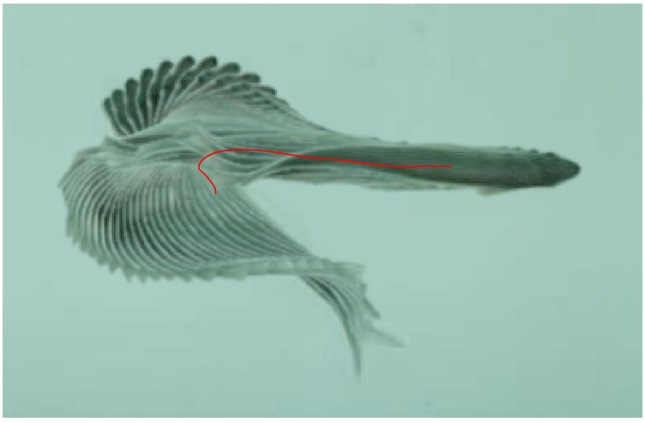

FIGURE 7 Centroid path for a tight turn [Color figure can be viewed at wileyonlinelibrary.com]

Whether our results generalize across body-caudal fin swimmers is unknown. The similarity in form between C-starts and routine maneuvers (Wu et al., 2007) and the ubiquity of C-starts in fishes suggests that this pattern persists across fish that use body-caudal-fin swimming. Similar curvature patterns have been reported in escape maneuvers in killifish (Fleuren et al., 2018) suggesting our results may hold more broadly. Morphological differences between fish will likely contribute to their maneuverability. Differences along the body-caudal fin spectrum may differ significantly in their control of turns, particularly at extreme ends of the spectrum. The fish we examined had less than one wave on their body at a time. Long undulating swimmers can have several bends on their bodies while navigating complex structure and may use different methods to control their turns. Conversely, stiff, thunniform swimmers would be limited in the range of body curvature they can develop on different regions of the body. This would reduce maneuverability (Blake et al., 1995; Domenici, 2001), and possibly be compensated for by other behaviors like using appendages (Fish, 1999), or high amplitude "ratcheting" turns (Downs et al., 2019). Fish that swim using their median and paired fins may use entirely different mechanisms to turn (Fish et al., 2018; Gerstner, 1999; Walker, 2000). Size limits absolute maneuverability, with larger animals having larger turning radii (Blake, 2004; Domenici, 2001; Vogel, 2008). As with stiffer fish, larger fish may rely on alternate behaviors to accomplish maneuvers outside of the range possible with a pulse behavior. As body size increases, inertia begins to dominate the animals hydrodynamic constraints. Larger animals are better able to take advantage of unpowered turns while smaller animals tend to rely on powered turns (Blake & Chan, 2006). Body postures and control of unpowered turns are likely to be different as animals are redirecting existing momentum as opposed to generating additional momentum.

Giant danios maneuver using a control scheme that unites the simplicity of their body plan with the complexity required to navigate their habitats. While fish have many possible ways to vary body curvature during propagating turns, only two main factors, the magnitude and duration of bending govern these changes. These two factors contribute to both of the turn outcome factors, the directional change (maneuverability) and the speeds and accelerations of the maneuver (agility). The overlap between factors allows fish the flexibility to use different combinations of midline curvature and duration to achieve similar whole-body outcomes. When individual pulses are insufficient to complete a desired maneuver, pulses can be combined to generate more complex maneuvers, accelerate more with a lower final heading change or achieve a desired heading change over a wider turn radius. The pulse model of fish turning also seamlessly integrates with general swimming mechanics and is seen in escape maneuvers, albeit in an altered form.

ACKNOWLEDGMENTS

The authors thank David Leffler for help gathering data, Dr. Brooke Flammang for help with project conceptualization, Dr. Peter Niewiarowski for help with statistical methods, and Dr. George Howe for inspiring a life long-love of the natural world, rest in peace.

https://datadryad.org/stash/share/wvYhEeXeJV85A5N8sdkOynDSyAzImFu2ji-On6ldGVI

CONFLICT OF INTERESTS

The authors declare that there are no conflict of interests.

ORCID

Stephen P. Howe http://orcid.org/0000-0003-0436-9078

Henry C. Astley https://orcid.org/0000-0003-0136-1433

REFERENCES

Akanyeti, O., Putney, J., Yanagitsuru, Y. R., Lauder, G. V., Stewart, W. J., & Liao, J. C. (2017). Accelerating fishes increase propulsive efficiency by modulating vortex ring geometry. *Proceedings of the National Academy of Sciences*, *114*(52), 13828–13833.

Biga, P. R., & Goetz, F. W. (2006). Zebrafish and giant danio as models for muscle growth: Determinate vs. indeterminate growth as determined by morphometric analysis. *American Journal of Physiology-Regulatory, Integrative and Comparative Physiology*, *291*(5), R1327–R1337. https://doi.org/10.1152/ajpregu.00905.2005

Blake, R. (2004). Fish functional design and swimming performance. *Journal of Fish Biology*, *65*(5), 1193–1222.

Blake, R., Chatters, L., & Domenici, P. (1995). Turning radius of yellowfin tuna (*Thunnus albacares*) in unsteady swimming manoeuvres. *Journal of Fish Biology*, *46*(3), 536–538.

Blake, R. W., & Chan, K. H. S. (2006). Models of the turning and fast-start swimming dynamics of aquatic vertebrates. *Journal of Fish Biology*, *69*(6), 1824–1836. https://doi.org/10.1111/j.1095-8649.2006.01251.x

Budick, S. A., & O'Malley, D. M. (2000). Locomotor repertoire of the larval zebrafish: Swimming, turning and prey capture. *Journal of Experimental Biology*, *203*(17), 2565–2579.

Chadwell, B. A., Standen, E. M., Lauder, G. V., & Ashley-Ross, M. A. (2012). Median fin function during the escape response of bluegill sunfish (*Lepomis macrochirus*). I: Fin-ray orientation and movement. The. *Journal of Experimental Biology*, *215*(16), 2869–2880. https://doi.org/10.1242/jeb.068585

Domenici, P. (2001). The scaling of locomotor performance in predator–prey encounters: From fish to killer whales. *Comparative Biochemistry and Physiology Part A: Molecular & Integrative Physiology*, *131*(1), 169–182.

Domenici, P., & Batty, R. S. (1994). Escape manoeuvres of schooling *Clupea harengus*. *Journal of Fish Biology*, *45*(sA), 97–110. https://doi.org/10.1111/j.1095-8649.1994.tb01086.x

Domenici, P., & Blake, R. (1997). The kinematics and performance of fish fast-start swimming. *Journal of Experimental Biology*, *200*(8), 1165–1178.

Domenici, P., & Blake, R. W. (1991). The kinematics and performance of the escape response in the Angelfish (*Pterophyllum Eimekei*). *Journal of Experimental Biology*, *156*(1), 187–205.

Domenici, P., & Blake, R. W. (1993). Escape trajectories in Angelfish (*Pterophyllum eimekei*). *The Journal of Experimental Biology*, *177*(1), 253–272.

Domenici, P., & Hale, M. E. (2019). Escape responses of fish: A review of the diversity in motor control, kinematics and behaviour. *The Journal of Experimental Biology*, *222*(18), jeb166009. https://doi.org/10.1242/jeb.166009

Domenici, P., Norin, T., Bushnell, P. G., Johansen, J. L., Skov, P. V., Svendsen, M. B. S., … Abe, A. S. (2015). Fast-starting after a breath: Air-breathing motions are kinematically similar to escape responses in the catfish *Hoplosternum littorale*. *Biology Open*, *4*(1), 79–85. https://doi.org/10.1242/bio.20149332

Domenici, P., Standen, E. M., & Levine, R. P. (2004). Escape manoeuvres in the spiny dogfish (*Squalus acanthias*). *Journal of Experimental Biology*, *207*(13), 2339–2349. https://doi.org/10.1242/jeb.01015

Downs, A. K. A., Block, B. A., & Fish, F. E. (2019). Turning performance by Bluefin Tuna: Novel mechanism for rapid maneuvers with a rigid body. *Society of Integrative and Comparative Biology*.

Dunn, T. W., Gebhardt, C., Naumann, E. A., Riegler, C., Ahrens, M. B., Engert, F., & Del Bene, F. (2016). Neural circuits underlying visually evoked escapes in larval zebrafish. *Neuron*, *89*(3), 613–628. https://doi.org/10.1016/j.neuron.2015.12.021

Eaton, R., DiDomenico, R., & Nissanov, J. (1988). Flexible body dynamics of the goldfish C-start: Implications for reticulospinal command mechanisms. *The Journal of Neuroscience*, *8*(8), 2758–2768. https://doi.org/10.1523/jneurosci.08-08-02758.1988

Eaton, R., Lee, R., & Foreman, M. (2001). The Mauthner cell and other identified neurons of the brainstem escape network of fish. *Progress in Neurobiology*, *63*(4), 467–485.

Eaton, R. C., DiDomenico, R., & Nissanov, J. (1991). Role of the Mauthner cell in sensorimotor integration by the brain stem escape network. *Brain, Behavior and Evolution*, *37*(5), 272–285.

Eaton, R. C., & Emberley, D. S. (1991). How stimulus direction determines the trajectory of the Mauthner-initiated escape response in a teleost fish. *Journal of Experimental Biology*, *161*(1), 469–487.

Eaton, R. C., Lavender, W. A., & Wieland, C. M. (1981). Identification of Mauthner-initiated response patterns in goldfish: Evidence from simultaneous cinematography and electrophysiology. *Journal of Comparative Physiology*, *144*(4), 521–531. https://doi.org/10.1007/bf01326837

Eaton, R. C., Nissanov, J., & Wieland, C. M. (1984). Differential activation of Mauthner and non-Mauthner startle circuits in the zebrafish: Implications for functional substitution. *Journal of Comparative Physiology A*, *155*(6), 813–820.

Fish, F. E. (1999). *Performance constraints on the maneuverability of flexible and rigid biological systems*. Paper presented at the International Symposium on Unmanned Untethered Submersible Technology, Autonomous Undersea Systems Institute, Durham New Hampshire.

Fish, F. E., Kolpas, A., Crossett, A., Dudas, M. A., Moored, K. W., & Bart-Smith, H. (2018). Kinematics of swimming of the manta ray: Three-dimensional analysis of open water maneuverability. *Journal of Experimental Biology*, *221*, jeb.166041.

Fleuren, M., van Leeuwen, J. L., Quicazan-Rubio, E. M., Pieters, R. P. M., Pollux, B. J. A., & Voesenek, C. J. (2018). Three-dimensional analysis of the fast-start escape response of the least killifish, *Heterandria formosa*. *The Journal of Experimental Biology*, *221*(7), https://doi.org/10.1242/jeb.168609

Foreman, M., & Eaton, R. (1993). The direction change concept for reticulospinal control of goldfish escape. *The Journal of Neuroscience*, *13*(10), 4101–4113.

Gerstner, C. L. (1999). Maneuverability of four species of coral-reef fish that differ in body and pectoral-fin morphology. *Canadian Journal of Zoology*, *77*(7), 1102–1110.

Ghisleni, G., Capiotti, K. M., Da Silva, R. S., Oses, J. P., Piato, Â. L., Soares, V., … Bonan, C. D. (2012). The role of CRH in behavioral responses to acute restraint stress in zebrafish. *Progress in Neuro-Psychopharmacology and Biological Psychiatry*, *36*(1), 176–182. https://doi.org/10.1016/j.pnpbp.2011.08.016

Gray, J. (1933). Directional control of fish movement. *Proceedings of the Royal Society of London. Series B, Containing Papers of a Biological Character*, *113*(781), 115–125.

Hale, M. E. (2002). S-and C-start escape responses of the muskellunge (*Esox masquinongy*) require alternative neuromotor mechanisms. *Journal of Experimental Biology*, *205*(14), 2005–2016.

Hill, A. V. (1938). The heat of shortening and the dynamic constants of muscle. *Proceedings of the Royal Society of London. Series B-Biological Sciences*, *126*(843), 136–195.

Howland, H. C. (1974). Optimal strategies for predator avoidance: The relative importance of speed and manoeuvrability. *Journal of Theoretical Biology*, *47*(2), 333–350.

Jayne, B. C., & Lauder, G. (1994). How swimming fish use slow and fast muscle fibers: Implications for models of vertebrate muscle recruitment. *Journal of Comparative Physiology A*, *175*(1), 123–131.

Jayne, B. C., & Lauder, G. V. (1993). Red and white muscle activity and kinematics of the escape response of the bluegill sunfish during swimming. *Journal of Comparative Physiology A*, *173*(4), 495–508. https://doi.org/10.1007/bf00193522

Langerhans, R. B. (2009). Trade-off between steady and unsteady swimming underlies predator-driven divergence in *Gambusia affinis*. *Journal of Evolutionary Biology*, *22*(5), 1057–1075.

Liu, Y. -C., & Hale, M. E. (2017). Local spinal cord circuits and bilateral mauthner cell activity function together to drive alternative startle behaviors. *Current Biology*, *27*(5), 697–704.

McClelland, J. (1839). Indian Cyprinidae. *Asiatic Researches*, 19), 217–471.

Meager, J. J., Domenici, P., Shingles, A., & Utne-Palm, A. C. (2006). Escape responses in juvenile Atlantic cod *Gadus morhua* L.: The effects of turbidity and predator speed. *Journal of Experimental Biology*, *209*(20), 4174–4184. https://doi.org/10.1242/jeb.02489

Moore, T. Y., & Biewener, A. A. (2015). Outrun or outmaneuver: Predator–prey interactions as a model system for integrating biomechanical studies in a broader ecological and evolutionary context. *Integrative and Comparative Biology*, icv074.

Norberg, U. M., & Rayner, J. M. (1987). Ecological morphology and flight in bats (Mammalia; Chiroptera): Wing adaptations, flight performance, foraging strategy and echolocation. *Philosophical Transactions of the Royal Society of London. B*, *316*(1179), 335–427.

Otsu, N. (1979). A threshold selection method from gray-level histograms. *IEEE Transactions on Systems, Man and Cybernetics*, *9*(1), 62–66.

Rome, L. C., Funke, R. P., Alexander, R. M., Lutz, G., Aldridge, H., Scott, F., & Freadman, M. (1988). Why animals have different muscle fibre types. *Nature*, *335*(6193), 824–827.

Schrank, A. J., Webb, P. W., & Mayberry, S. (1999). How do body and paired-fin positions affect the ability of three teleost fishes to maneuver around bends? *Canadian Journal of Zoology*, *77*(2), 203–210.

Schriefer, J. E., & Hale, M. E. (2004). Strikes and startles of northern pike (*Esox lucius*): A comparison of muscle activity and kinematics between S-start behaviors. *Journal of Experimental Biology*, *207*(3), 535–544. https://doi.org/10.1242/jeb.00789

Tytell, E. D., & Lauder, G. V. (2002). The C-start escape response of *Polypterus senegalus*: Bilateral muscle activity and variation during stage 1 and 2. *Journal of Experimental Biology*, *205*(17), 2591–2603.

Tytell, E. D., & Lauder, G. V. (2008). Hydrodynamics of the escape response in bluegill sunfish, *Lepomis macrochirus*. *Journal of Experimental Biology*, *211*(21), 3359–3369. https://doi.org/10.1242/jeb.020917

Voesenek, C. J., Pieters, R. P. M., Muijres, F. T., & van Leeuwen, J. L. (2019). Reorientation and propulsion in fast-starting zebrafish larvae: An inverse dynamics analysis. *The Journal of Experimental Biology*, *222*(14), jeb203091. https://doi.org/10.1242/jeb.203091

Vogel, S. (2008). Modes and scaling in aquatic locomotion. *Integrative and Comparative Biology*, *48*(6), 702–712. https://doi.org/10.1093/icb/icn014

Wakeling, J. M., & Johnston, I. A. (1998). Muscle power output limits fast-start performance in fish. *Journal of Experimental Biology*, *201*(10), 1505–1526.

Walker, J. A. (2000). Does a rigid body limit maneuverability? *Journal of Experimental Biology*, *203*(22), 3391–3396.

Webb, P. W. (1976). The effect of size on the fast-start performance of rainbow trout Salmo gairdneri, and a consideration of piscivorous predator-prey interactions. *The Journal of Experimental Biology*, *65*(1), 157–177.

Webb, P. W. (1978). Fast-start performance and body form in seven species of Teleost fish. *The Journal of Experimental Biology*, *74*(1), 211–226.

Webb, P. W. (1983). Speed, acceleration and manoeuvrability of two teleost fishes. *Journal of Experimental Biology*, *102*(1), 115–122.

Webb, P. W. (1994). The biology of fish swimming, *Mechanics and physiology of animal swimming* (pp. 45–62). Cambridge: Cambridge University Press.

Webb, P. W., & Fairchild, A. G. (2001). Performance and maneuverability of three species of teleostean fishes. *Canadian Journal of Zoology*, *79*(10), 1866–1877.

Webb, P. W., & Skadsen, J. M. (1980). Strike tactics of Esox. *Canadian Journal of Zoology*, *58*(8), 1462–1469. https://doi.org/10.1139/z80-201

Weihs, D. (1973). The mechanism of rapid starting of slender fish. *Biorheology*, *10*(3), 343–350.

Westneat, M. W., Hale, M. E., McHenry, M. J., & Long, J. H. (1998). Mechanics of the fast-start: Muscle function and the role of intramuscular pressure in the escape behavior of *Amia calva* and *Polypterus palmas*. *Journal of Experimental Biology*, *201*(22), 3041–3055.

Wilson, A. M., Hubel, T. Y., Wilshin, S. D., Lowe, J. C., Lorenc, M., Dewhirst, O. P., … Golabek, K. A. (2018). Biomechanics of predator–prey arms race in lion, zebra, cheetah and impala. *Nature*, *554*(7691), 183–188.

Wilson, A. M., Lowe, J., Roskilly, K., Hudson, P. E., Golabek, K., & McNutt, J. (2013). Locomotion dynamics of hunting in wild cheetahs. *Nature*, *498*(7453), 185–189.

Wu, G., Yang, Y., & Zeng, L. (2007). Routine turning maneuvers of koi carp *Cyprinus carpio* koi: Effects of turning rate on kinematics and hydrodynamics. *Journal of Experimental Biology*, *210*(24), 4379–4389. https://doi.org/10.1242/jeb.009787

SUPPORTING INFORMATION

Additional supporting information may be found online in the Supporting Information section.

How to cite this article: Howe SP, Astley HC. The control of routine fish maneuvers: Connecting midline kinematics to turn outcomes. *J Exp Zool*. 2020;1–16. https://doi.org/10.1002/jez.2398